

PACS numbers: 52.57.–z; 52.50.Jm; 52.30.–q
DOI: 10.1070/QE2013v043n05ABEH015020

Simulations of thermal wave propagation in a target irradiated by high-intensity p-polarised laser radiation*

V.Yu. Politov

Abstract. **In a one-dimensional hydrodynamic approximation the evolution of a hot dense plasma produced by a high-power subpicosecond laser pulse absorbed primarily due to the resonance mechanism is investigated numerically. The heated plasma parameters of light and heavy chemical elements are compared. A prediction is made concerning the feasibility of producing a thin uniform plasma layer of a heavy substance in experiments on the irradiation of compound targets.**

Keywords: *subpicosecond laser pulse, thermal wave, p polarisation, resonance absorption.*

1. Introduction

The rapid progress of high-power laser systems capable of generating ultrashort pulses ranging from a fraction of a picosecond to several picoseconds in duration and having intensities ranging up to and exceeding the relativistic limit $10^{18}-10^{19}$ W cm^{-2} gives impetus to computational-theoretical investigations in the area of such high-intensity radiation–matter interaction. Interest is generated primarily in the processes responsible for the conversion of optical photon energy to fast particle and X-ray fluxes.

The most consistent approach to the simulation of the set of these complex energy processes relies on the 'particle-in-cell' (PIC) mathematical technique. This technique implies the solution of the equations of motion for electron and ion plasma components in self-consistent electric and magnetic fields. It permits taking into account in the general case the real three-dimensional experiment geometry, the nonuniformity of laser irradiation, the non-Maxwellian particle velocity distribution, etc. However, the software implementation of the PIC model calls for extremely large computational resources and does not guarantee against the emergence of numerical instabilities associated with the spatial separation of electric charges. Being kinetic in its nature, the particle technique is not optimal for the description of thermodynamic plasma properties in high-density domains, where the dominant role is played by particle collisions rather than interactions with the fields.

The hydrodynamic direction of high-intensity process simulations in laser plasmas also remains topical. Even in the simplest approximation of one-dimensional geometry, with the help of hydrodynamic models it is possible to estimate the significant characteristics of such plasmas like the expanding plasma density profile, the velocity and penetration depth of a thermal wave in the solid-density region, and the ionisation multiplicity. In this case, the computational burden is by far lighter than with the use of PIC codes.

In the present work we outline a version of such a hydrodynamic model oriented primarily to the description of the interaction of a laser target with p-polarised radiation incident at some angle to its normal. The specific character of this irradiation generates a need for taking into account the electric plasma charge wave, its influence on the steepening of expanding plasma density profile due to the action of the ponderomotive force and the conversion of a fraction of laser pulse energy to fast electrons (resonance absorption).

Considering all these effects, a numerical investigation was made of target heating depth in relation to the chemical target composition. These simulations were made for irradiation conditions typical for experiments on the SOKOL-P high-power picosecond facility [1].

2. Model of p-polarised radiation–matter interaction

The hydrodynamic description of the interaction of ultrashort laser pulses with matter involves the combined solution of electrodynamic equations for laser field components as well as the equations of motion and heat transfer in the plasma produced in the absorption of the field energy. The specific form of these equations depends on several assumptions about the geometry of laser target irradiation, the radiation intensity, the type of polarisation, the method of including the ionisation of atomic shells in the plasma energy balance, X-ray photon transfer, etc. By way of example of the implementation of suchlike hydrodynamic models, mention can be made of Refs [2, 3] concerned with the description of the plasma dynamics of spherical fusion targets and the two-dimensional expansion of planar foils in intense laser fields with the inclusion of the resonance absorption mechanism of light energy.

Without going into the complexities of multidimensional behaviour of the plasma medium, we restrict ourselves to planar irradiation approximation, when the laser beam incident (in the general case, obliquely) on the target is focused to a uniform spot with a diameter far greater than the target thick-

*Presented at the Laser Optics Conference, St. Petersburg, Russia, June 2012.

V.Yu. Politov E.I. Zababakhin All-Russian Scientific-Research Institute of Technical Physics, Russian Federal Nuclear Centre, ul. Vasil'eva 13, 456770 Snezhinsk, Chelyabinsk region, Russia; e-mail: v_politov@mail.ru

Received 15 October 2012; revision received 23 December 2012
Kvantovaya Elektronika **43** (5) 449–457 (2013)
Translated by E.N. Ragozin

ness. When the radiation is p-polarised, its field is characterised by two electric components, $\boldsymbol{E} = (E_x, E_y, 0)$, one of which is oriented along the normal to the focal spot and the other lies in its plane (the x- and y-directions), as well as by magnetic field $\boldsymbol{H} = (0, 0, H_z)$ orthogonal to the $\boldsymbol{E}$ vector. Since the pulse front is assumed to be plane, all field components and their related currents have the form of waves with the frequency ω_0 of laser radiation travelling in the y direction:

$$E_x, E_y, H_z \sim [E_x(x), E_y(x), H_z(x)]\exp(\mathrm{i}k_0 y\sin\theta_0 - \mathrm{i}\omega_0 t), \quad (1)$$

where $k_0 = \omega_0/c$ is the vacuum wave number; θ_0 is the angle of radiation incidence on the target; and c is the speed of light. From this equation it follows that the laser energy density $Q_E \sim |\boldsymbol{E}|^2$ absorbed in the target depends only on the x coordinate. Therefore, it reasonable to assume that during irradiation all hydrodynamic processes in the target material, including heat propagation from the absorption region, proceed unidimensionally in the direction normal to focal plane. The effects of side expansion of the heated plasma at the boundaries of irradiation region are neglected. This formulation is employed to advantage in the simulation of experiments in a broad range of peak intensities $I_0 \leqslant 10^{17}$ W cm^{-2} of laser pulses (mostly s-polarised), when the effect of light pressure may be neglected (see, for instance, Refs [4–6]).

2.1. Electrodynamic equations

We precede from the general Maxwell equations in the frequency representation to derive the equations describing the spatial amplitudes $E_x(x)$, $Ey(x)$ and $H_z(x)$ (in what follows the argument x will be omitted) of monochromatic p-polarised electromagnetic field with the oscillating time dependence $\sim\exp(-\mathrm{i}\omega_0 t)$:

$$\mathrm{rot}\boldsymbol{E} = \mathrm{i}\frac{\omega_0}{c}\boldsymbol{H}, \qquad \mathrm{rot}\boldsymbol{H} = \frac{4\pi}{c}\boldsymbol{j} - \mathrm{i}\frac{\omega_0}{c}\boldsymbol{E}, \quad (2)$$

where $\boldsymbol{j} = (j_x, j_y, 0)$ is the density of the total electric current, which is the superposition of polarisation and conduction currents.

To define these relations concretely, the currents j_x, j_y should be expressed in terms of the intensities of the electric components E_x and E_y. In the model of continuous media this is accomplished with the complex permittivity tensor, which is characterised by the diagonal components ε_x, ε_y in the one-dimensional geometry selected. The difference between these components is determined by the different character of energy exchange between the field and the target substance in the x and y directions. In the target plane the E_y field component gives rise to forced electron oscillations, whose energy dissipates only in collisions with the resultant plasma particles. In the normal direction the E_x field generates a plasma wave, which gives rise to macroscopic charge separation. In this case, the dissipation of electron oscillation energy takes place both due to interparticle interactions and a collisionless mechanism, which is responsible for the generation of fast electrons. In strong fields the collisionless dissipation frequency, which has the meaning of a Landau damping frequency ν_L, may exceed the frequency ν_T of collisional processes for thermal electrons. Furthermore, owing to charge separation there emerges an additional thermal contribution j_T to the conduction current [7], tending to decrease this separation, which in turn results in the limitation of the magnitude of the plasma field and in its partial 'ejection' from the domain of laser pulse absorption to the vacuum region. Therefore, the currents along the y and x directions may be represented as

$$j_y = -\mathrm{i}\omega_0\frac{\varepsilon_y - 1}{4\pi}E_y, \qquad j_x = -\mathrm{i}\omega_0\frac{\varepsilon_x - 1}{4\pi}E_x + j_T. \quad (3)$$

The rigorous definition of permittivity tensor components for a plasma with sharp density gradients, which result in the spatial dispersion, anisotropy, and the smearing of plasma wave spectrum, is a separate complex mathematical problem, whose solution calls for applying the methods of multigroup kinetic theory. That is why, focusing on the hydrodynamic description of target substance behaviour, which evolves from the cold state to a strongly heated and highly ionised state, there is good reason to employ a simple wide-range phenomenological expression:

$$\varepsilon_{x,y} = 1 - \frac{\omega_\mathrm{p}^2}{\omega_0^2 + \nu_{x,y}^2} + \mathrm{i}\frac{\nu_{x,y}}{\omega_0}\frac{\omega_\mathrm{p}^2}{\omega_0^2 + \nu_{x,y}^2}, \quad (4)$$

where $\nu_y = \nu_T$ and $\nu_x = \nu_T + \nu_\mathrm{L}$. This expression takes into account the effect of plasma waves by one, inherently phenomenological parameter ν_L/ω_0. This expression coincides in form with the Drude formula for metals and reproduces the fraction of optical energy absorbed in the target with a reasonable accuracy with the proviso that $\nu_\mathrm{L} \ll \nu_T$ [5, 6]. The quantity ω_p, which enters in expression (4), is the plasma oscillation frequency defined, like in Ref. [8], with correction for the increase in electron mass m_e in a laser field with intensity exceeding the relativistic threshold, I_rel [W cm^{-2}] = $1.23 \times 10^{18}/\lambda_0^2$ [μm]:

$$\omega_\mathrm{p} = \sqrt{\frac{4\pi e^2 Z_\mathrm{p}\rho}{mM}}, \quad (5)$$

where

$$m = m_\mathrm{e}\sqrt{1 + \frac{c\,|\boldsymbol{E}|^2\varphi(t)}{8\pi I_\mathrm{rel}}};$$

e is the electron charge; Z_p and M are the average charge and mass of target ions; ρ is the plasma density; $\lambda_0 = 2\pi/k_0$ is the radiation wavelength; and $\varphi(t)$ is the time function of the laser pulse defined in the form of a triangle, whose peak value is equal to unity at the point in time coinciding with the pulse duration.

The relation between the current j_T and the field E_x is found in the framework of the clear analytical treatment, which was outlined in monograph Ref. [9], of one-dimensional electron oscillations heated to a temperature T_e under the action of this field and intrinsic pressure gradient. In the hydrodynamic approximation it turns out that this current is proportional to the density gradient of the electron fraction which makes up the plasma charge uncompensated by the ions: $j_T \sim \partial n_\mathrm{e}/\partial x$. The density of the electrons is found from the solution of one-dimensional Poisson equation $\partial E_x/\partial x = -4\pi e n_\mathrm{e}(x)$. Solving the equation of oscillatory motion under the specified assumptions and excluding the density $n_\mathrm{e}(x)$ from it yields the net result:

$$j_T = -\mathrm{i}\omega_0\frac{\beta}{4\pi k_0^2}\frac{\partial^2 E_x}{\partial x^2}, \quad (6)$$

where

$$\beta = \frac{\beta_T}{1 + \mathrm{i}v_x/\omega_0}; \quad \beta_T = \frac{3T_\mathrm{e}}{m_\mathrm{e}c^2}.$$

Under this approach we simultaneously obtain an estimate for the collisionless damping frequency of the plasma wave

$$\frac{v_\mathrm{L}}{\omega_0} \sim \left(\frac{\beta_T}{k_0^2 L^2}\right)^{1/3}, \tag{7}$$

which has correct asymptotic limits: $v_\mathrm{L} \to 0$ in the cold substance ($T_\mathrm{e} \to 0$) and $v_\mathrm{L} \to \infty$ when the plasma nonuniformity length L tends to zero (for a step-like vacuum–plasma interface).

Substitution of the wave dependences (1) and relations (3), (6) in the vector Maxwell equations leads to a system of three interrelated equations:

$$\begin{aligned}
&\frac{\beta}{k_0^2}\frac{\partial^2 E_x}{\partial x^2} + \varepsilon_x E_x = -\sin\theta_0 H_z,\\
&\frac{\partial}{\partial x}\left(\frac{\varepsilon_x}{\varepsilon_x - \sin^2\theta_0}\frac{\partial E_y}{\partial x}\right) + k_0^2 E_y \varepsilon_y\\
&\quad = \mathrm{i}\frac{\partial}{k_0 \partial x}\left(\frac{\beta \sin\theta_0}{\varepsilon_x - \sin^2\theta_0}\frac{\partial^2 E_x}{\partial x^2}\right),\\
&\frac{\partial}{\partial x}\left(\frac{1}{\varepsilon_y}\frac{\partial H_z}{\partial x}\right) + k_0^2 H_z\left(1 - \frac{\sin^2\theta_0}{\varepsilon_x}\right) = \frac{\beta \sin\theta}{\varepsilon_x}\frac{\partial^2 E_x}{\partial x^2}.
\end{aligned} \tag{8}$$

The coefficients in these equations depend on the state of the material medium and are described in terms of parameters ε_x, ε_y, and β. The effect of factor β, which is always much smaller than unity in magnitude, manifests itself only in a narrow spatial region near the point of field reflection, where the real parts of the permittivity tensor components vanish and the derivative $\partial^2 E_x/\partial x^2$ is large.

It needs to define the boundary conditions for system (8). The laser radiation in a vacuum is initially assumed to have the form of a plane travelling wave

$$E_0 \exp[-\mathrm{i}\omega_0 t + \mathrm{i}k_0(\cos\theta_0 x + \sin\theta_0 y)],$$

incident on the target from left to right at an angle θ_0 to the normal; $E_0 = [8\pi I_0 \varphi(t)/\mathrm{c}]^{1/2}$ is the amplitude of this wave. Then all components of the total field on the left of the target, which is made up of the incident and reflected waves, should satisfy the following relations at some point x_1 in vacuum:

$$\begin{aligned}
&\left(\frac{\partial \boldsymbol{E}}{\partial x} + \mathrm{i}k_0 \cos\theta_0 \boldsymbol{E}\right)\Big|_{x_1} = 2\mathrm{i}k_0 E_0 \exp(\mathrm{i}k_0 \cos\theta_0 x_1) \times\\
&\quad \times(\cos\theta_0 \sin\theta_0, \cos^2\theta_0, 0),\\
&\left(\frac{\partial H_z}{\partial x} + \mathrm{i}k_0 \cos\theta_0 H_z\right)\Big|_{x_1} = 2\mathrm{i}k_0 E_0 \exp(\mathrm{i}k_0 \cos\theta_0 x_1)\cos\theta_0.
\end{aligned} \tag{9}$$

At the rear side of a sufficiently thick target, the field may be assumed to be zero.

2.2. Equations of plasma heating and motion

The generation of currents by a high-power laser pulse in the surface layer of the substance under irradiation leads to a rapid transition of this substance to the plasma state as well as to the production of a fast electron flux at the vacuum boundary. These high-energy electrons propagate virtually instantly deep into the target, because their mean free path is much longer than for thermal electrons. The charge they take away is compensated for by reverse currents, whose energy density is negligible in comparison with the density of absorbed pulse energy. Therefore, the fast electrons are included in the model only as a factor which lowers the rate of surface plasma heating.

The direct action of laser radiation on this plasma is described using a system of hydrodynamic equations, which is subdivided into two groups for convenience of numerical implementation: thermal equations and equations of motion. In the limiting case of ultrashort irradiation (tens of femtoseconds) the plasma may at all be treated as immobile owing to the inertia of ions. However, when the pulse duration amounts to a fraction of a picosecond or to several picoseconds the plasma motion may no longer be neglected. The initially step-like target density profile acquires a tailing over such periods of time, which may have a significant effect on the absorption of pulse energy.

The thermal equations are written relative to the temperatures T_e, T_i of the electron and ion subsystems of the plasma jointly with an additional equation describing the evolution of the average charge Z_p of its constituent ions, which may markedly differ from the equilibrium value $Z_\mathrm{p,eq}$ under subpicosecond heating (especially for heavy substances):

$$\begin{aligned}
&C_{V\mathrm{e}}\left(\frac{\partial T_\mathrm{e}}{\partial t} + V\frac{\partial T_\mathrm{e}}{\partial x}\right) = Q_E - (P_\mathrm{e} + P_V)\frac{\partial V}{\partial x} - \frac{\partial q_T}{\partial x} - Q_\mathrm{ei} - Q_\mathrm{ion},\\
&C_{V\mathrm{i}}\left(\frac{\partial T_\mathrm{i}}{\partial t} + V\frac{\partial T_\mathrm{i}}{\partial x}\right) = Q_\mathrm{ei} - P_\mathrm{i}\frac{\partial V}{\partial x},\\
&\frac{\partial Z_\mathrm{p}}{\partial t} + V\frac{\partial Z_\mathrm{p}}{\partial x} = J\left(1 - \frac{Z_\mathrm{p}}{Z_\mathrm{p,eq}}\right).
\end{aligned} \tag{10}$$

Here, Q_E, Q_ion, and Q_ei are the specific (per unit volume of the substance) powers of the thermal absorption of laser photons, ionization of target atoms, and electron-ion exchange; q_T is the thermal flux density; $C_{V\mathrm{e}}$, $C_{V\mathrm{i}}$, P_e, and P_i are the specific heat capacities and pressures of the electron and ion subsystems; P_V is the artificial quadratic viscosity of the substance defined by the velocity profile $V(x)$ of hydrodynamic motion [10]; and J is the collisional ionization rate. We neglect the energy loss due to the intrinsic radiation of the heated layer, because it is assumed that particle collisions prevail over photoprocesses in solid-density plasmas. Of course, for relativistic laser intensities $I_0 > 10^{18}$ W cm^{-2}, which correspond to high ($T_\mathrm{e} > 1$ keV) heating temperatures, this assumption is not obvious and calls for a special investigation. We also neglect the ion conduction flux.

The expressions for heat capacities, pressures, exchange term, and the electron flux are taken from Ref. [6]:

$$\begin{aligned}
&P_\mathrm{e} = \frac{Z_\mathrm{p}\rho}{M}T_\mathrm{e}, \quad P_\mathrm{i} = \frac{\rho}{M}T_\mathrm{i},\\
&C_{V\mathrm{e}} = \frac{3Z_\mathrm{p}\rho}{2M}\frac{T_\mathrm{e}}{T_\mathrm{e} + 3T_\mathrm{F}/\pi^2}, \quad C_{V\mathrm{i}} = \frac{3\rho}{2M},
\end{aligned} \tag{11}$$

$$Q_\mathrm{ei} = 3Z_\mathrm{p}\frac{m_\mathrm{e}\rho}{M^2}\nu_T(T_\mathrm{e} - T_\mathrm{i}), \tag{12}$$

$$q_T = -\frac{128}{3\pi}\frac{Z_\mathrm{p}\rho T_\mathrm{e}}{M m_\mathrm{e}\nu_T}\frac{\partial T}{\partial x}.$$

In this case, the ions are treated as an ideal gas irrespective of the density and the temperature. The effect of degeneracy on C_{Ve} in included for electrons in the cold parts of the target with a temperature below the Fermi temperature T_F. The electron–ion collision frequency, which enters in the definitions of the energy quantities Q_E, Q_{ei}, and q_T, is also corrected in relation to the temperature range. For $T_e \to \infty$ the frequency v_T is defined by the Spitzer formula [11] and for $T_e \to 0$ the frequency is estimated proceeding from the notions of electron-phonon interactions [12]:

$$v_T = \begin{cases} \dfrac{4\sqrt{2}\,e^4}{3M\sqrt{m_e}}\dfrac{Z_p\rho}{T_e^{3/2}}\Lambda_e, & T_e > T_F, \\ \dfrac{T_i}{\hbar}\left(1+\dfrac{T_e^2}{T_F T_i}\right), & T_e \leqslant T_F, \end{cases} \qquad (13)$$

where h is Planck's constant; and

$$\Lambda_e = \ln\left(1 + 9\frac{MT_e^3}{4\pi\rho Z_p^3 e^6}\right)$$

is the Coulomb logarithm for weakly nonideal plasmas.

We shall enlarge on the expressions for the terms responsible for the absorption of the laser pulse energy and plasma ionisation. With the use of the complex parts of permittivity tensor components (4), the absorption power takes the form of the sum of the contributions generated by fields E_x, E_y:

$$Q_E = I_0\varphi(t)k_0\omega_p^2\frac{v_T}{\omega_0}\left(\frac{|E_y/E_0|^2}{\omega_0^2+v_T^2} + \frac{|E_x/E_0|^2}{\omega_0^2+(v_T+v_L)^2}\right). \qquad (14)$$

Calculations suggest that, despite the fact that the plasma wave escapes to the vacuum region (low-density substance region) and the transfer of the bulk of energy to fast electrons, its contribution to the Q_E quantity may prevail.

The formula for ionisation loss follows from the equation for average ion charge evolution and from the definition of the specific internal energy of thermal electrons in the limit of ideal gas (neglecting low-temperature degeneracy) $W_e = \rho(1.5Z_pT_e + U(Z_p))/M$:

$$Q_{ion} = J\frac{\rho}{M}\left(1-\frac{Z_p}{Z_{p,eq}}\right)\left(U(Z_p)+\frac{3}{2}T_e\right), \qquad (15)$$

where $U(Z_p)$ is the energy required to detach Z_p bound electrons from a target atom. For an arbitrary chemical element this energy is calculated by the algorithm of piecewise-linear interpolation [13] between the ionisation potentials U_k of the ion ground states for all k integer multiplicities – from the neutral atom to the fully ionised state with charge equal to the nuclear charge $Z_p = Z_0$ of the element. The discrete potentials U_k themselves are found using spectroscopic codes in the Hartree–Fock–Slater approximation [14].

Proceeding from the functional dependence $U(Z_p)$ and the known thermodynamic plasma parameters, it is also possible to estimate the collisional ionisation rate by the semiempirical Seaton formula [15]:

$$J = \frac{4\sqrt{\pi}\,ca_B^2}{137M}N(Z_p)\rho Z_p\frac{Ry^{3/2}}{\sqrt{T_e\,U(Z_p)}}\exp\left(-\frac{U(Z_p)}{T_e}\right), \qquad (16)$$

where $Ry = 0.0136$ keV; a_B is the Bohr radius; and $N(Z_p)$ is the average number of equivalent ionisable electrons in the ground state of the ion of charge $\sim Z_p$. The number N is found, like the average ionisation potential, using an interpolation algorithm. We add that the factor $1 - Z_p/Z_{p,eq}$, which corrects the rate J in the ionisation equations, takes into account three-body recombination, which manifests itself most significantly at the stage of plasma expansion and cooling after the laser pulse action. The value of equilibrium charge $Z_{p,eq}$, which enters in this factor, is found from the Saha model [16].

The mechanism of collisional ionisation determines the evolution of the average plasma ion charge in the overcritical high-density region and, as a consequence, affects the velocity of thermal wave propagation into the target. However, in the subcritical region the efficiency of this process is much lower (the value of J is smaller), and the ion composition of the plasma is affected by the tunnel ionisation of atomic shells by the electric field of the laser wave, which is taken into account like in Ref. [12]. The external field of intensity $|\boldsymbol{E}|$ lowers the potential barrier, which prevents the bound electrons from transiting to the free state, by a value $\Phi \sim 2e(eZ_p|\boldsymbol{E}|)^{1/2}$. This leads us to assume that all electrons from shells with $U_k < \Phi$ are instantaneously ionised. This assumption results in an implicit expression for Z_p in a given external field:

$$Z_p \sim \frac{U^2(Z_p)}{4e^2\sqrt{|E_x|^2+|E_y|^2}}. \qquad (17)$$

We next turn to the formulation of the equations of plasma motion. The first equation is a conventional continuity equation, which relates the hydrodynamic parameters ρ and V in a differential form, the second one represents the momentum conservation law and may have different representations. In the selection of the specific representation, first of all we take into account the special character of the interaction of high-intensity laser radiation with a solid substance. For relativistic intensity values $I_0 \geqslant I_{rel}$ the ponderomotive pressure P_E in the absorption region may exceed the total material pressure $P = P_e + P_i + P_V$ and impede the expansion of the heated plasma, maintaining a very steep density gradient at the boundary under irradiation. To minimise the influence of this gradient on the accuracy of numerical solutions, the momentum equation for the plasma medium is conveniently transformed to the form containing only a weak logarithmic density function, considering that all types of pressure depend linearly on ρ in high-temperature plasmas. Finally the equations of motion are represented as follows:

$$\frac{\partial\rho}{\partial t} = -\frac{\partial}{\partial x}(\rho V),$$
$$\frac{\partial V}{\partial t} = -\frac{\partial}{\partial x}\left(\frac{V^2}{2}+\frac{P}{\rho}+\frac{P_E}{\rho}\right) - \frac{P}{\rho}\frac{\partial\ln\rho}{\partial x}, \qquad (18)$$

where the ponderomotive pressure is defined by the expression [12]

$$P_E = \frac{e^2Z_p\rho}{4m_eM\omega_0^2}(|E_x|^2+|E_y|^2). \qquad (19)$$

The relativistic increase in electron mass is neglected in this expression.

2.3. Numerical implementation of the model

The numerical integration of the model equations with respect to time from the onset of irradiation is performed in three stages on a common immobile Eulerian grid. At the first

stage, the sweep method is used to solve the stationary field equations for the thermodynamic parameters known from the previous time step. The equation of electron heat transfer is solved jointly with the equations of ion heating and ionisation by an implicit scheme, which is second-order accurate in space and first-order accurate in time, with the known electric field distributions $E_x(x)$ and $E_y(x)$. In doing this, advantage is taken of complete linearisation technique with the use of Newtonian iterations in electron temperature, whose number is controlled by a preset convergence criterion. At the last stage, new values of the density and velocity of hydrodynamic plasma motion are calculated by an explicit scheme, the velocity being determined in the middle of the intervals of the spatial cells. The length of time steps is selected using an adaptive algorithm, which controls the maximum admissible variations of T_e within the computational domain.

In view of the effect of a very strong ponderomotive pressure, an accurate reproduction of a virtually step-like plasma density profile in the solution of model equations results in the generation of a very small time step – no longer than $(2-3)\times 10^{-4}$ ps. As a consequence, $\sim 10^4$ steps fall within a time interval approximately equal to the picosecond pulse duration. The spatial grid must also be sufficiently fine, especially so in the pulse absorption domain. It was experimentally determined that the results of simulations became almost insensitive to spatial discretisation when the interval Δx in this domain did not exceed $(2-5)\times 10^{-3}$ μm. For the grid dimension not to be too large (and hence for the problem computation time not to be too long), use is made of an algorithm for lengthening the grid intervals to values of the order of those in the vacuum domain and the domain of thermal wave propagation through the cold substance. For a target several micrometres in thickness, the characteristic number of spatial mesh nodes is equal to 500–1000. The $x = 0$ coordinate corresponds to the exterior boundary of the substance in the initial (cool) state.

3. Model testing

The stated model was tested using the data of experiments, which are recognised as benchmark experiments, on the ultrashort-pulse irradiation of solid targets of different materials [17, 18] for moderate intensities ($I_0 < 10^{16}$ W cm^{-2}). In these experiments the laser photon reflection coefficients from the resultant plasma were measured as functions of irradiation angle θ_0 and the magnitude of I_0. The quality of target fabrication (the surface polishing) made it possible to reduce to almost zero the diffuse scattering. As a result, almost all reflected radiation energy was recorded in the mirror direction relative to the irradiation direction. This reflection corresponds to the boundary conditions (9) for electromagnetic fields and must be adequately described by a one-dimensional hydrodynamic model.

The mathematical determination of the absorbed and reflected energy fractions may be performed on the basis of the system of equations (8). Additional complex-conjugate equations are formulated for both components of the electric field. Then the initial equations are multiplied by intensities E_x^*, E_y^* and the conjugate ones by E_x, E_y. In this case, in the right-hand side of the equation for E_y we neglect the small contribution from the plasma wave current ($j_T \sim \beta_T \ll 1$). Upon integration of the resultant relations over the entire computation domain, the subsequent pairwise subtraction, the use of Maxwell's equations (2) and the boundary conditions, and some transformations of the left- and right-hand sides, there emerges a standard relation between the absorption and reflection coefficients:

$$A = 1 - R. \tag{20}$$

The expression for the reflection coefficient R at each point in time is consistent with the requirement of superposition of the incident and reflected waves of the electric field at the left boundary of the computation domain with coordinate x_1:

$$R = 1 + \frac{|E_x(x_1)|^2 + |E_y(x_1)|^2}{E_0^2}$$

$$- \frac{2}{E_0}\mathrm{Re}\{\exp(-\mathrm{i}k_0 x_1 \cos\theta_0)[\cos\theta_0 E_y(x_1) - \sin\theta_0 E_x(x_1)]\}. \tag{21}$$

The absorption coefficient A is the sum of the contributions, A_T and A_F, of thermal and fast electrons:

$$A_T = \frac{k_0}{\cos\theta_0}\int \mathrm{d}x \omega_p^2 \frac{\nu_T}{\omega_0}\left(\frac{|E_y/E_0|^2}{\omega_0^2 + \nu_T^2} + \frac{|E_x/E_0|^2}{\omega_0^2 + (\nu_T + \nu_L)^2}\right),$$

$$A_F = \frac{k_0}{\cos\theta_0}\int \mathrm{d}x \frac{\nu_L}{\omega_0}\left(\frac{\omega_p^2 |E_x/E_0|^2}{\omega_0^2 + (\nu_T + \nu_L)^2} + \beta\left|\frac{\partial(E_x/E_0)}{\partial x}\right|^2\right). \tag{22}$$

For comparison with experimental data, the quantities R, A_T, and A_F should be averaged over the time law of laser pulse intensity variation:

$$\bar{A}_{T,F} = \frac{\int \mathrm{d}t\varphi(t) A_{T,F}(t)}{\int \mathrm{d}t\varphi(t)}, \quad \bar{R} = \frac{\int \mathrm{d}t\varphi(t) R(t)}{\int \mathrm{d}t\varphi(t)}. \tag{23}$$

These averaged coefficients were calculated on completion of the simulation of the spatiotemporal evolution of the laser target plasma over a pre-assigned time interval. The initial point in time $t_0 = 0$ corresponds to the onset of the laser pulse $\varphi(t_0) = 0$. The target is assumed to be in one of two states at this point in time: it is either a cool solid substance with a step-like density profile and a known Fermi temperature or an expanding preplasma with a pre-assigned gradient scale length and a seed free-electron density preformed at the vacuum interface.

The absorption and reflection coefficients were primarily simulated for the experimental conditions of Ref. [17], in which the Al target was irradiated both by p- and s-polarised radiation at an angle $\theta_0 = 45°$ for $I_0 = 10^{11} - 10^{16}$ W cm^{-2} for a wavelength $\lambda_0 = 0.3$ μm and a laser pulse duration $\tau_0 = 0.4$ ps. The possible effect of a weak prepulse irradiation was neglected. The Fermi temperature of cool aluminium $T_F \sim 11$ eV, which permits estimating the initial charge of metallic plasma: $Z_p(t_0) \sim 2.5$ (the Fermi surface in metals was assumed to be spherically shaped). The initial electron temperature corresponded to the room one: $T_e(t_0) = T_i(t_0) = 0.025$ eV. The electron–phonon collision frequency was selected proceeding from the known thermal conductivity coefficient of aluminium of 2.4 J s^{-1} cm^{-1} K^{-1}.

The calculated dependence of the total absorption coefficient $\bar{A} = \bar{A}_T + \bar{A}_F$ on the peak intensity, which exceeds 5×10^{12} W cm^{-2}, is compared with the experimental values of $1 - R_{exp}$ in Fig. 1a. In view of the measurement uncertainty estimated at 5%–10%, it is safe to say that the quantities under comparison are in reasonable agreement with each other. For low I_0 values (no greater than 10^{12} W cm^{-2}) this agreement is missing, because the model does not take into

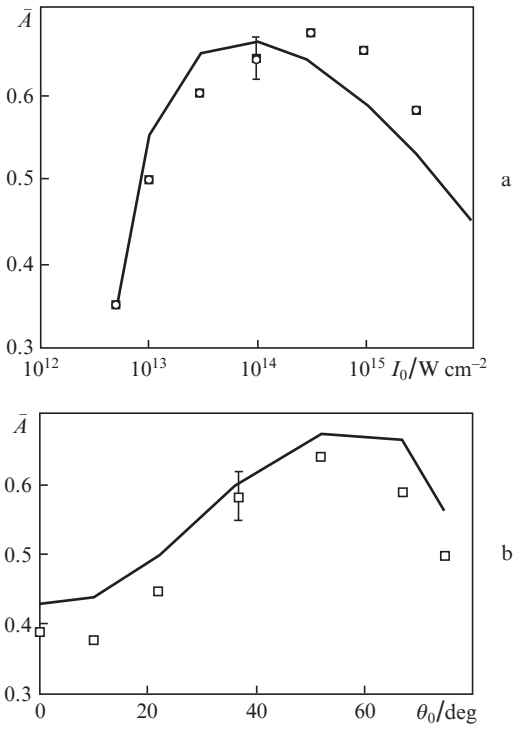

Figure 1. Dependences of the absorption coefficient of a p-polarised laser pulse in Al on the peak irradiation intensity for $\lambda_0 = 0.3$ μm, $\tau_0 = 0.4$ ps, $\theta_0 = 45°$ (a) and on the angle of irradiation for $\lambda_0 = 0.25$ μm, $\tau_0 = 0.25$ ps, $I_0 = 10^{14}$ W cm^{-2} (b). The points represent the experimental data of Refs [17, 18].

account the mechanism of interband absorption of optical photons in a low-temperature plasma, when $T_e < T_F$.

We also investigated the absorbed energy dependences on the angle of Al target irradiation for a constant I_0 value. The irradiation parameters were taken the same as in Ref. [18]: $I_0 = 10^{14}$W cm^{-2}, $\lambda_0 = 0.25$ μm, and $\tau_0 = 0.25$ ps. A comparison of the calculated and experimental data (Fig. 1b) testifies that their disagreement also does not exceed 10% for the majority of angles θ_0.

Therefore, test simulations suggest that, beginning from $I_0 \sim 10^{16}$ W cm^{-2}, the absorption of p-polarised laser radiation is primarily due to the resonance mechanism, which is responsible for the generation of a fast electron flux.

4. Results of thermal wave simulations in different substances

As noted above, the main applications of the hydrodynamic model and its software implementation are aimed at analysing the feasibility of producing in high-intensity laser experiments thin uniform plasma layers that are uniform in temperature and density. For this purpose a series of simulations was performed for targets of different chemical composition under irradiation conditions typical for the SOKOL-P high-power laser facility: wavelength $\lambda_0 = 1.05$ μm, $I_0 = 10^{18} - 10^{19}$ W cm^{-2}, $\tau_0 = 0.7$ ps. The level of contrast ratio achieved on this facility so far does not permit eliminating prepulses with energies sufficient for plasma production on the target surface under irradiation. However, the solution of this problem is in sight. That is why the prepulses were disregarded in the simulations outlined (although this possibility has been built into the model) and the initial target state at the onset of the main pulse was treated as a solid one with a step-like boundary. It is precisely the absence of a boundary plasma cloud that is an important condition to efficient laser energy transfer from the absorption region to the unperturbed inner regions.

The angle of incidence of p-polarised radiation is $\theta_0 = 45°$. The substances under irradiation were polyethylene (CH) and gold, which have substantially different initial densities ($\rho_0 =$ 1 and 19.6 g cm^{-3}) and ionisation energies of their constituent atoms. The layer thicknesses of these substances were selected from the condition that the thermal wave does not manage to reach the rear side of the target. Owing to the difference in ionisation expenses the light target must evidently warm up faster than the heavy one. Furthermore, the lower the average plasma charge, the higher the electron thermal conductivity coefficient. That is why in our simulations the thickness of the CH layer was set equal to 2.5 μm and that of the Au layer to 1 μm. Formulation of the boundary conditions for electric field intensities required that a 1.5-μm thick vacuum region with a background gas density of 10^{-10} g cm^{-3} was located in front of the target.

Our simulation data suggest that the spatial field distributions are hardly dependent on the chemical target composition and are immune to variations over a wide range (0.5–2) of the plasma wave damping parameter ν_L/ω_0 during target irradiation by a pulse with $I_0 \geqslant I_{rel}$. Figure 2 shows examples of the field distribution at the moment the pulse with $I_0 = 10^{18}$ W cm^{-2} reaches its peak. Also shown in Fig. 2 is the profile of normalised plasma frequency; it takes into account the cloud of electrons at the target boundary under irradiation, which oscillate along the x direction [19]. Such a cloud formation is a kinetic effect and may only approximately be described in the framework of a hydrodynamic model – for instance, by continuous distribution of electrons, which are ejected from the target surface, over a domain of length of the order of the oscillation amplitude $r_{os} \sim e|\bar{E}x|/\sqrt{2}\, m_x\omega_0^2$, where $\bar{E}x$ is some average field intensity of the plasma wave. The oscillation charge separation included in this way, like the relativistic increase in electron mass, manifests itself only in a displacement of the field reflection point and has only an insignificant effect on the general dynamics of the plasma layer.

The spatial behaviour of the most important hydrodynamic parameters T_e and ρ/ρ_0 for the CH and Au targets, which was simulated in the course of combined solution with the field equations, is depicted in Figs 3 and 4 for several char-

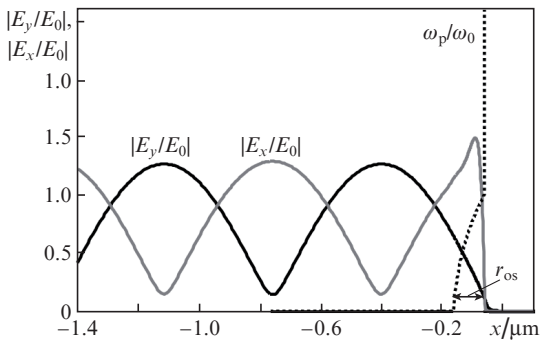

Figure 2. Normalised electric field intensities and normalised plasma frequency at the instant of peak irradiation for $\lambda_0 = 1.05$ μm, $\tau_0 = 0.7$ ps, $\theta_0 = 45°$, and $I_0 = 10^{18}$ W cm^{-2}.

acteristic points in time during irradiation by the laser pulse and after its end. One can see from these dependences that the ponderomotive pressure strongly prevents the plasma expansion of the light substance, in which the ionised electron density, and hence the thermal pressure, are much lower than in the heavy substance. Furthermore, at the peak of irradiating pulse intensity the light substance begins to compress rather than expand.

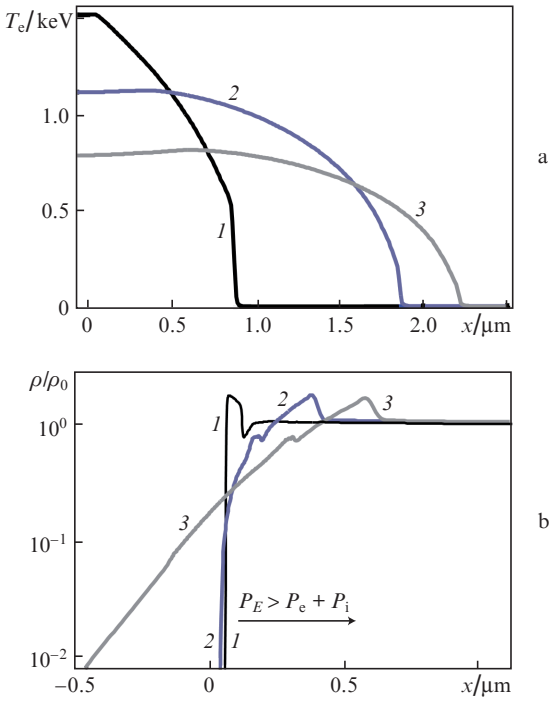

Figure 4. Spatial distributions of the electron temperature (a) and density (b) in the Au plasma at the points in time $t = 0.7$ (*1*), 1.4 (*2*), and 2 ps (*3*) for a laser target thickness of 1 μm.

Figure 3. Spatial distributions of the electron temperature (a) and density (b) in the CH plasma at the points in time $t = 0.7$ (*1*), 1.4 (*2*), and 2 ps (*3*) for a laser target thickness of 2.5 μm.

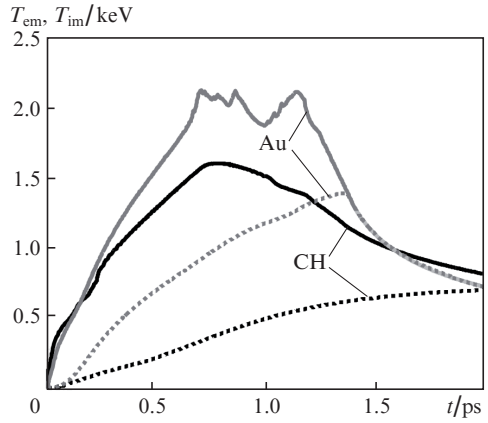

Figure 5. Highest temperatures of the electron (solid curves) and ion (dotted lines) components of the CH and Au plasmas.

The redistribution of thermal energy also proceeds differently in the targets under consideration. Owing to a relatively low ionisation loss the thermal wave in the CH plasma overtakes the density perturbation wave, and a density-uniform heated layer may exist for several picoseconds. The thickness of this layer with a temperature $T_e \geqslant 1$keV is estimated at no less than 1 μm and with $T_e \sim 0.5$ keV at 2 μm. For a heavy substance like gold the situation is different. In this case, the propagation of an electron thermal conduction wave is slowed down by multiple ionisation, which is responsible for the growth of the average plasma charge and, therefore, for the rise of its thermal resistance. The calculated depth of Au target heating does not exceed 0.2–0.4 μm, appreciable distortions of the initial density profile simultaneously appearing at this depth, so that the plasma layer may not be treated as a uniform one during any time interval. The highest attainable values of the electron and ion temperatures, T_{em} and T_{im}, as well as estimates of their equalising time are given in Fig. 5 for both targets.

The correctness of the combined solution of electrodynamic and hydrodynamic equations is checked by the accuracy to which the total energy conservation law is fulfilled for the system under irradiation, on the one hand, and by the balance of laser photon absorption and reflection coefficients, on the other. The calculated time dependences of the A_T, A_F, and R coefficients are plotted in Fig. 6 for CH and Au. They testify that the balance relation (20) is fulfilled to an accuracy of 5%–10% during the course of the pulse. According to our numerical analysis, the discrepancy appears primarily due to the ponderomotive steepening of the density profile. To eliminate it requires too fine a spatial mesh in the E_x field–plasma interaction region. The thermal absorption coefficients averaged over the pulse duration are $\bar{A}_{T\mathrm{CH}} \sim 0.024$ and $\bar{A}_{T\mathrm{Au}} \sim 0.083$. The bulk of absorbed energy is expended to generate fast electrons, which is estimated a $\bar{A}_F \sim 0.35$–0.4. This value is in reasonable agreement with the data of recent experiments [20] carried out on the CALLISTO laser facility in Lawrence Livermore National Laboratory. In the irradiation

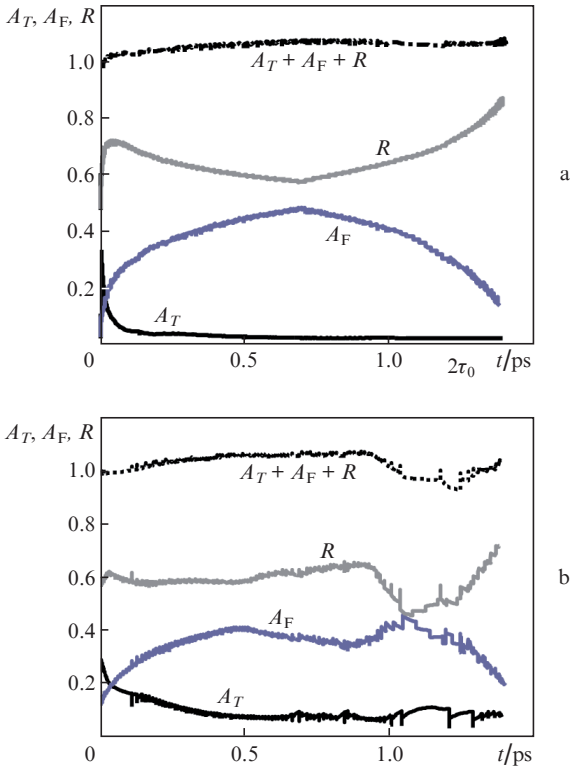

Figure 6. Absorption and reflection coefficients for the CH (a) and Au (b) plasmas during the course of a p-polarised laser pulse with $I_0 = 10^{18}$ W cm^{-2}.

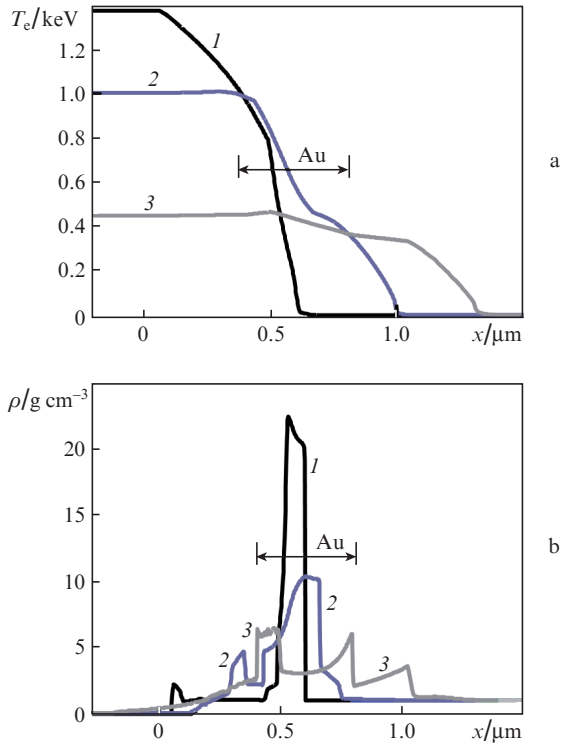

Figure 7. Spatial distributions of the electron temperature (a) and normalised density (b) at the points in time $t = 0.7$ (*1*), 1.4 (*2*), and 2 ps (*3*) in the plasma of the three-layer target, where a 0.1-μm thick Au layer is between a 0.5-μm thick external CH layer and a 1.5-μm thick rear CH layer.

of aluminium foils by pulsed 0.15-ps p-polarised radiation at a wavelength of 0.8 μm, the total laser energy absorption coefficient was equal to 0.4–0.6 in the peak intensity range $I_0 = 10^{17}$–10^{19} W cm^{-2}.

Endeavours to improve the uniformity of heavy substance plasma layer in conditions of ultrashort laser irradiation leads to the concept of a compound target, when a heavy substance is screened from direct irradiation by a light substance, which decreases density perturbations and forms a thermal wave. In the simulation of the heating dynamics of the compound target it was assumed that a 0.1-μm thick gold layer is covered with polyethylene layers with respective thicknesses of the external and rear layers of 0.5 and 1.5 μm, respectively. Examples of the spatial T_e and ρ distributions in the resultant multilayer plasma are given in Fig. 7. They suggest that the Au layer temperature equalization sets in only after the end of the laser pulse, at the points in time $t > 2$ ps, when the thermal wave nearly stops and its temperature decreases from the maximum value of 1.5 keV to ~0.4 keV. At these instants of time, the Au plasma pressure exceeds the pressure in the CH cover layers (the ionisation multiplicity is higher), with the consequential broadening of the heavy layer and a several-fold lowering of its density, down to $\rho \sim 3 - 4$ g cm^{-3}. Figure 8 shows the distributions of the average ion charge for $t = 0.7$ and 2.4 ps. A comparison of these distributions with the equilibrium ones shows that an equality $Z_p = Z_{p,eq} = 3.5$ is fulfilled in the heated CH light layers, while the equilibrium charge state approximation breaks down in the heavy layer. The difference between Z_p and $Z_{p,eq}$ ranges up to a factor of two, which must have a significant effect on the dynamics of the plasma as a whole, because $P_e \sim Z_p$. The inertia of ionisation and recombination maintains the value of Z_p in the heated Au layer at about a constant level in the 40–50 range.

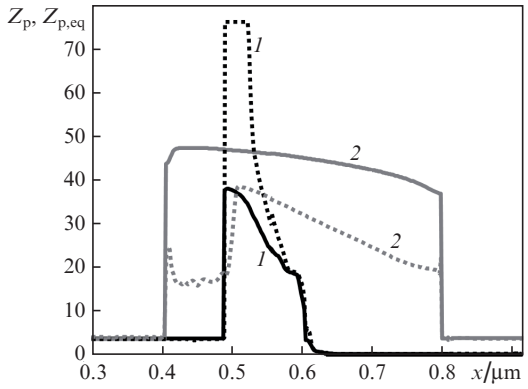

Figure 8. Nonequilibrium (solid curves) and equilibrium (dotted lines) average ion charges in the layered plasma at the point in time $t = 0.7$ (*1*) and 2.4 ps (*2*).

5. Conclusions

We presented the results of numerical simulations of the interaction of high-power p-polarised ultrashort-pulse laser radiation with single-and multilayer targets consisting of light and heavy substances (polyethylene and gold) for a peak irradiation intensity $I_0 \sim I_{rel}$. The objective of our simulations was to determine the depth of thermal wave penetration into solid

media which require substantially different energy expenses for the ionisation of electron shells.

The simulations were performed in the framework of a one-dimensional hydrodynamic model, which described the heating, ionisation, and motion of the substance in a strong light field. These simulations included the effects of ponderomotive pressure and transfer of a part of laser pulse energy to the energy of fast electrons by means of a damping plasma wave generated by the external field in the normal direction to the target plane.

The model equations were numerically implemented on a common Eulerian grid. The integration scheme was second-order approximative in space and first-order approximative in time. The energy balance equation for the plasma produced in the absorption of laser photons is implicitly solved relative to the thermal electron temperature involving iterations in nonlinearities and automatic time step selection. The equations of motion are solved using an explicit algorithm.

A conclusion was drawn from the simulations that the thermal wave intensity in light substances is sufficient for producing for several picoseconds a density-uniform high-temperature plasma layer 1–2 μm in thickness. In the case of heavy substances, multiple ionisation prevents the thermal wave from detaching the shock one, which disturbs the uniformity of the plasma and permits heating it to a depth of no more than a fraction of a micrometer. Hence it follows that a more or less uniform plasma layer of a heavy substance may be produced if it is screened from the direct ponderomotive action by a rapidly heated layer of a light substance. The heavy layer thickness must be considerably less that 1 μm.

It is planned to verify the model predictions using the data of X-ray measurements in dedicated experiments on the SOKOL-P facility for irradiation intensities above 10^{18} W cm^{-2}. To this end, the model should be complemented with a software module intended to construct the X-ray emission spectra of dense layered plasmas. Furthermore, it needs to take into account, at least in the Rosseland length approximation, the energy fraction carried away by this radiation.

References

1. Potapov A.V., Loboda E.A., Politov V.Yu., et al. *Fiz. Plazmy*, **33**, 3 (2007).
2. Afanas'ev Yu.V., Gamalii E.G., Demchenko N.N., et al. *Zh. Eksp. Teor. Fiz*., **79**, 837 (1980).
3. Lebo I.G., Demchenko N.N., Iskakov A.B., et al. *Laser Part. Beams*, **22**, 267 (2004).
4. Price D.F., More R.M., Walling R.S., et al. *Phys. Rev. Lett*., **75** (2), 252 (1995).
5. Velichko V.M., Urlin V.D., Yakutov B.P. *Kvantovaya Elektron*., **30**, 889 (2000) [*Quantum Electron*., **30**, 889 (2000)].
6. Eidmann K., Meyer-ter-Veln J., Schlegel T. *Phys. Rev. E*, **62**, 1202 (2000).
7. Forslund D.W., Kindel J.M., Kenneth Lee, et al. *Phys. Rev. A*, **11**, 679 (1975).
8. Hora H. *Physics of Laser-Driven Plasmas* (New York: Wiley, 1981; Moscow: Energoatomizdat, 1986).
9. Ginzburg V.L. *The Propagation of Electromagnetic Waves in Plasmas* (Oxford: Pergamon Press, 1970; Moscow: Fizmatgiz, 1960).
10. Samarskii A.S., Popov Yu.P. *Raznostnye skhemy gazovoi dinamiki* (Difference Schemes of Gas Dynamics) (Moscow: Nauka, 1975).
11. Spitzer L. *Physics of Fully Ionized Gas* (New York: Interscience Publ., 1956).
12. Andreev N.E., Veisman M.E., Efremov V.P., et al. *Teplofiz. Vys. Temp*., **41**, 679 (2003).
13. Zel'dovich Ya.B., Raizer Yu.P. *Physics of Shock Waves and High-Temperature Hydrodynamic Phenomena* (New York: Academic Press, 1966, 1967; Moscow: Nauka, 1966).
14. Cowan R.D. *The Theory of Atomic Structure and Spectra* (Berkley: University of California Press, 1981).
15. Vainshtein L.A., Shevel'ko V.P. *Struktura i kharakteristiki ionov v goryachei plazme* (Structure and Characteristics of Ions in Hot Plasmas) (Moscow: Nauka, 1986).
16. Nikiforov A.F., Novikov V.G., Uvarov V.B. *Kvantovo-statisticheskie modeli vysokotemperaturnoi plazmy* (Quantum-Statistical Models of High-Temperature Plasma) (Moscow: Fizmatlit, 2000).
17. Milchberg H.M., Freeman R.R., Davey S.C., et al. *Phys. Rev. Lett.*, **61**, 2364 (1988).
18. Fedosejevs R., Ottman R., Sigel R., et al. *Phys. Rev. Lett*., **64**, 1250 (1990).
19. Brunnel F. *Phys. Rev. Lett*., **59**, 52 (1987).
20. Ping Y., Sheperd R., Lasinski B.F., et al. *Phys. Rev. Lett*., **100**, 085004 (2008).